

Broadband electroluminescence from reverse breakdown in individual suspended carbon nanotube pn-junctions

© Tsinghua University Press and Springer-Verlag GmbH Germany, part of Springer Nature 2020 **Received:** 14 November 2019 / Revised: 6 June 2020 / Accepted: 19 June 2020

ABSTRACT

There are various mechanisms of light emission in carbon nanotubes (CNTs), which give rise to a wide range of spectral emission characteristics that provide important information regarding the underlying physical processes that lead to photon emission. Here, we report spectra obtained from individual suspended CNT dual-gate field effect transistor (FET) devices under different gate and bias conditions. By applying opposite voltages to the gate electrodes (i.e., $V_{g1} = -V_{g2}$), we are able to create a pn-junction within the suspended region of the CNT. Under forward bias conditions, the spectra exhibit a peak corresponding to E₁₁ exciton emission via thermal (i.e., blackbody) emission occurring at electrical powers around 8 μ W, which corresponds to a power density of approximately 0.5 MW/cm². On the other hand, the spectra observed under reverse bias correspond to impact ionization and avalanche emission, which occurs at electrical powers of ~ 10 nW and exhibits a featureless flat spectrum extending from 1,600 nm to shorter wavelengths up to 600 nm. Here, the hot electrons generated by the high electric fields (~ 0.5 MV/cm) are able to produce high energy photons far above the E₁₁ (ground state) energy. It is somewhat surprising that these devices do not exhibit light emission by the annihilation of electrons and holes under forward bias, as in a light emitting diode (LED). Possible reasons for this are discussed, including Auger recombination.

KEYWORDS

ballistic, avalanche, high-field, band-to-band, photoemission

1 Introduction

Our ability to control, produce, and enhance light emission from carbon nanotubes (CNTs) is based largely on photoluminescence measurements in which an intense laser is used to photoexcite the nanotubes. Over the past ten years, several research groups have reported that oxygen doping of CNTs using ozonolysis produces localized exciton states, which exhibit long photoluminescence lifetimes (> 1 ns), enhanced photoluminescence intensities ($\sim 20\times$), and promising $g^{(2)}$ -factors up to room temperature [1-11]. Kato's group recently reported single photon emission at room temperature from air-suspended CNTs [12]. Prior to these studies, however, single photon emission in carbon nanotubes and other nanoscale materials (quantum dots, TMDCs) had been relegated to cryogenic temperatures [9, 13, 14]. Hogele et al. demonstrated that carbon nanotubes emit non-classical light at 4.2 K through the observation of photon antibunching in the photoluminescence of a suspended single carbon nanotube [9]. This was the first report of quantum correlations of photoemission in a single CNT, and the probability of multiphoton emission was found to be smaller than 3%, indicating that carbon nanotubes could be used as a source of single photons for applications in quantum cryptography and quantum information processing. Strauf's group also observed photon antibunching with $g^2(0) = 0.15$ from cavity-embedded (6,5) CNTs dispersed in a sodium dodecylsulfate (SDS) solution at 9 K [14]. It should be noted, however, that in these previous studies light emission was produced by optical pumping.

While the study of optically-pumped light emission from CNTs has evolved to an unprecedented level of control and sophistication, electrically-driven light emission from individual carbon nanotubes has lagged way behind. Early reports of electroluminescence (EL) from individual carbon nanotube devices around the early 2000s included several papers from the IBM group, who reported an electroluminescence efficiency of $\sim 10^{-4}$ photons per injected electron-hole pair [15, 16]. Typical electrical powers dissipated in these devices (P = IV) were on the order of 10s of μW [16–22]. While several mechanisms of light emission have been discussed in these early EL studies, including electron-hole annihilation and impact ionization, it is likely that the main mechanism of emission in these early studies was from thermal emission due to substantial heating. At these applied powers, substantial Joule heating occurs as evidenced by monitoring the G band shift in their Raman spectra [20, 21, 23-25]. As a result, thermal emission caused by heating (~ 1,000 K) is likely the main mechanism of light emission occurring in these previous works.

¹ Department of Physics and Astronomy, University of Southern California, Los Angeles, CA 90089, USA

² Ming Hsieh Department of Electrical Engineering, University of Southern California, Los Angeles, CA 90089, USA

³ Mork Family Department of Chemical Engineering and Materials Science, University of Southern California, Los Angeles, CA 90089, USA

⁴ Center for Integrated Nanotechnologies, Materials Physics and Applications Division, Los Alamos National Laboratory, Los Alamos, NM 87545, USA

In 2018, avalanche photoemission was reported from individual suspended carbon nanotubes under large applied electric fields, resulting in efficient generation of light without heat at applied electrical powers of just 4 nW [21, 22]. This corresponds to unipolar light emission, thus circumventing the difficulty associated with injecting electrons into CNTs due to their small electron affinities and large associated Schottky barriers. Thermal emission by Joule heating was ruled out by Raman spectroscopy, however, no spectral characterization was done of this avalanche photoemission process.

In the work presented here, we have recorded the light emission spectra from suspended dual-gate CNT field effect transistor (FET) devices under both forward and reverse bias conditions. Here, we are able to tune through various mechanisms of light emission from thermal emission to impact ionization and, eventually, avalanche electroluminescence. In addition to the spectral profiles, we compare the relative electroluminescence efficiencies of these two basic emission mechanisms.

Figure 1(a) shows a diagram of the dual-gate CNT FET device. In the microfabrication process, a pair of 100 nm thick platinum gate electrodes are first deposited on an undoped Si substrate using photolithography and electron-beam metal deposition. A 600-nm thick SiO₂ layer is then deposited using plasma enhanced chemical vapor deposition (PECVD). A trench is etched through the SiO₂ layer approximately 1 µm wide and 600-nm deep using reaction ion etching (RIE). Photolithography is then used to pattern 29 pairs of platinum source and drain electrodes on top of the SiO₂ layer with 100 nm in thickness. The gap between the source and drain electrodes is 2 µm, and the gap between the two gates is 200 nm. Figure 1(b) shows a scanning electron microscope (SEM) image of a suspended CNT across a pair of source and drain electrodes. Figure 1(c) shows optical microscope images of a typical dual-gate CNT FET chip [26–28]. Catalyst windows (5 μ m × 5 μ m) are patterned in a photoresist layer on top of the source and drain electrodes near the trench enabling us to deposit ferric nitrate Fe(NO₃)₃/ Al₂O₃-based catalyst. The final step of the sample fabrication process is chemical vapor deposition (CVD) of CNTs at 825 °C by bubbling hydrogen and argon gas through pure ethanol [29]. For the electrical characterization of these devices, a semiconductor parameter analyzer (HP, Inc) is used. EL images are collected with a thermoelectrically-cooled InGaAs camera (Xenics, Inc) with a 1,100-1,600 nm effective wavelength range. EL spectra are collected using a homebuilt spectrometer system with a liquid nitrogen-cooled InGaAs array (Princeton Instrument, Inc) over the same effective wavelength range.

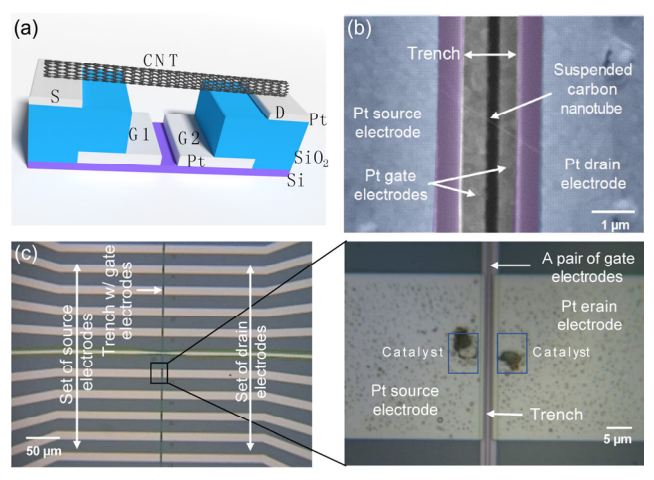


Figure 1 (a) Schematic diagram, (b) SEM image, and (c) optical microscope images of a dual-gate, partially suspended carbon nanotube FET.

The current-gate voltage $(I-V_g)$ characteristics of a suspended dual-gate CNT FET device are plotted in Fig. 2(a). Here, the two gates are shorted together and a constant bias voltage +0.2 V was applied (i.e., single-gate configuration). This $I-V_g$ curve indicates that this is an ambipolar device with a charge neutral point at $V_g = 1.75$ V. However, the contact resistance associated with n-type conduction ($V_g = +10 \text{ V}$) is approximately 1,000× higher than that of p-type conduction ($V_g = -10 \text{ V}$). Figure 2(b) shows the current plotted as a function of bias voltage obtained by setting the two gate voltages to equal and opposite values of $V_{g1} = -V_{g2} = 10$ V, which results in the formation of a pn-junction within the CNT. By reversing the gate voltages, we can achieve reversible rectifying behavior, indicating that the rectifying behavior is not simply due to one of the Schottky contacts associated with the Pt/CNT junction. Calculated conduction and valence band profiles of a dual-gate CNT FET device showing the formation of pn-junctions at (a) $V_{\rm gl} = -V_{\rm g2} =$ -15 V and (b) $V_{g1} = -V_{g2} = 15 \text{ V}$ under a bias voltage of 3 V are shown in Fig. S2 in the Electronic Supplementary Material (ESM). Figure 2(c) shows the electric current and the EL intensity plotted together as a function of bias voltage while gating another device in the np-configuration (i.e., $V_{\rm gl} = -V_{\rm g2} = +10$ V). Under forward bias, the current increases abruptly above $V_b >$ 0.5 V, however, electroluminescence is not observed until $V_b >$ 2 V when the current is above 2 μ A. This corresponds to a

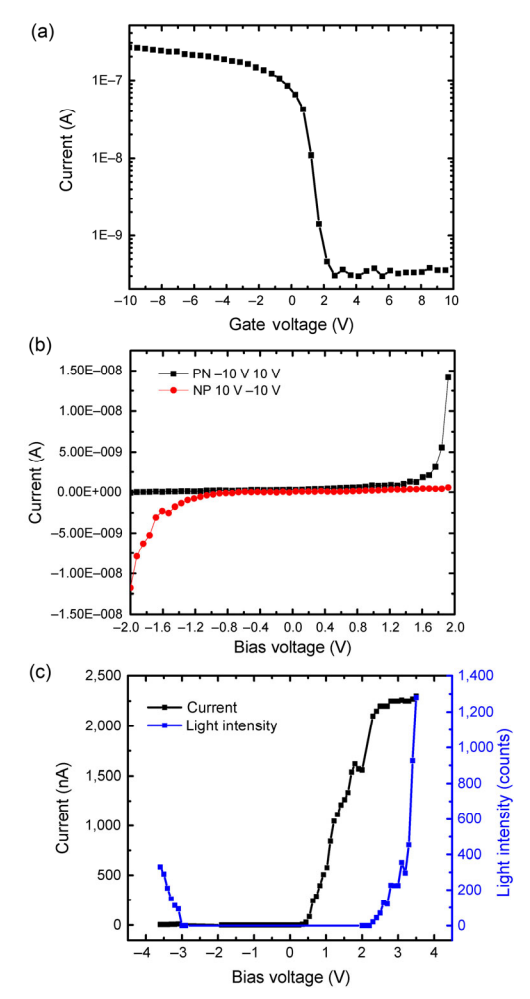


Figure 2 (a) Current-gate voltage (I–V_g) characteristics measured from a suspended dual-gate CNT FET device obtained by shorting the two gates (i.e., $V_{\rm g1} = V_{\rm g2}$) and applying a constant bias voltage of 0.2 V. (b) Current plotted as a function of bias voltage by gating the device in the pn (V_{g1} = -10 V and $V_{g2} = 10 \text{ V}$) and np ($V_{g1} = 10 \text{ V}$ and $V_{g2} = -10 \text{ V}$) configurations. (c) Current and EL intensity plotted as a function of bias voltage at $V_{\rm gl}$ =

regime in which the electrical power exceeds 4 μ W and light emission occurs via thermal emission. Under reverse bias, we observe light emission for bias voltages below -3 V with currents less than 4 nA (P=12 nW), which corresponds to the sub-avalanche regime in which light emission occurs via impact ionization. This avalanche behavior is described in detail in our previous papers [21, 22, 30]. Here, we should note that while the electric current remains almost a constant in the reverse biased region, the light emission intensity increases sharply with the increase of the bias voltage. This occurs because the increased bias voltage leads to a higher electric field, which enhances the impact ionization emission of light.

The thermal emission spectrum taken under forward bias $(V_b = 3.5 \text{ V}, I_b = 2.3 \mu\text{A}, P = 8 \mu\text{W})$ is plotted in Fig. 3(a) and exhibits a wide peak corresponding to a thermally-broadened E₁₁ exciton transition. For most of our devices, the typical electrical power required for thermal emission to reach the light detection limit of our optical system is approximately 3 μW. Photoluminescence (PL) spectra taken from two representative dual-gate CNT FETs are plotted in Fig. S1 in the ESM. Figure 3(b) shows the spectrum of sub-avalanche light emission taken under reverse bias at $V_b = -3.6 \text{ V}$ and $I_b = 4 \text{ nA}$ (P =14.4 nW), which exhibits a flat spectrum extending significantly beyond the ground state E11 transition. Here, sub-avalanche light emission occurs at relative light emission efficiency (EL intensity/electric power) that is 150× higher than thermal emission. It is somewhat surprising that these devices do not exhibit light emission under lower forward bias currents (< 1 μA) by the annihilation of electrons and holes, as in a light emitting diode (LED). One possible reason for this is the high nonradiative recombination rates in the nanotubes, as evidenced by the relatively high reverse saturation currents, which are typically above 1 nA [31]. Auger recombination, which is a non-radiative process, is another possible mechanism by which the light emission efficiency is reduced by more than one order of magnitude at high gate voltages [32-35]. Also, the high n-type contact resistances, which result in a substantial voltage drop across the contact instead of the pn-junction itself. Figures 3(c) and 3(d) show visible-light-range spectra of thermal emission and sub-avalanche light emission collected from another dual gate CNT FET device using a silicon CCD detector. Figure 3(c) shows the spectrum of thermal emission taken in the forward biased region at $V_b = 3.7$ V and $I_b = 2.0$ μ A (P = 7.4 μ W), which exhibits a peak around 785 nm, corresponding to a thermally-broadened E22 exciton feature. Figure 3(d) shows the spectrum of sub-avalanche light emission taken under reverse bias at $V_b = -3.8$ V and $I_b = 4$ nA (P = 15.2 nW), which exhibits a featureless flat spectrum. Here, again, sub-avalanche light emission also exhibits a much higher ($\sim 200\times$) relative light emission efficiency (EL intensity/electric power) than that of thermal emission within the visible wavelength range.

Photon emission from avalanche breakdown in silicon was reported in 1956 by Chynoweth and McKay. In this work, photon emission up to 3.2 eV was observed from a silicon pn-junction under reverse bias [36]. This is almost three times higher than the band gap energy of silicon, which exemplifies how electrons accelerating in high electric fields can gain enough kinetic energy to emit photons many times greater than the band gap (or ground state) energy (i.e., E₁₁ exciton in the case of a CNT) of a material. More recently, van Drieënhuizen et al. reported simulations of above-band gap emission in avalanche-mode silicon pn-junctions under high fields (~ 10⁵ V/cm) [37]. In carbon nanotubes, however, electrons can accelerate in these high fields without scattering because of the limited number of scattering states in k-space that conserve momentum. That is, CNTs provide a unique one-dimensional system in which phonon scattering is suppressed, enabling hot electrons to emit high energy photons.

In conclusion, we report spectra obtained from individual suspended CNT pn-junction devices under forward and reverse bias. Under forward bias, the spectra exhibit a relatively inefficient thermal emission peak centered around the E_{11} exciton at electrical powers of approximately 8 μW . Under reverse bias, however, we observe efficient broadband emission extending up to wavelengths as short as 600 nm corresponding to impact ionization and avalanche emission, at electrical powers of ~ 10 nW. These devices do not exhibit light emission by the annihilation of electron and holes under forward bias, as occurs in LEDs, indicating high non-radiative recombination rates possibly due to Auger recombination.

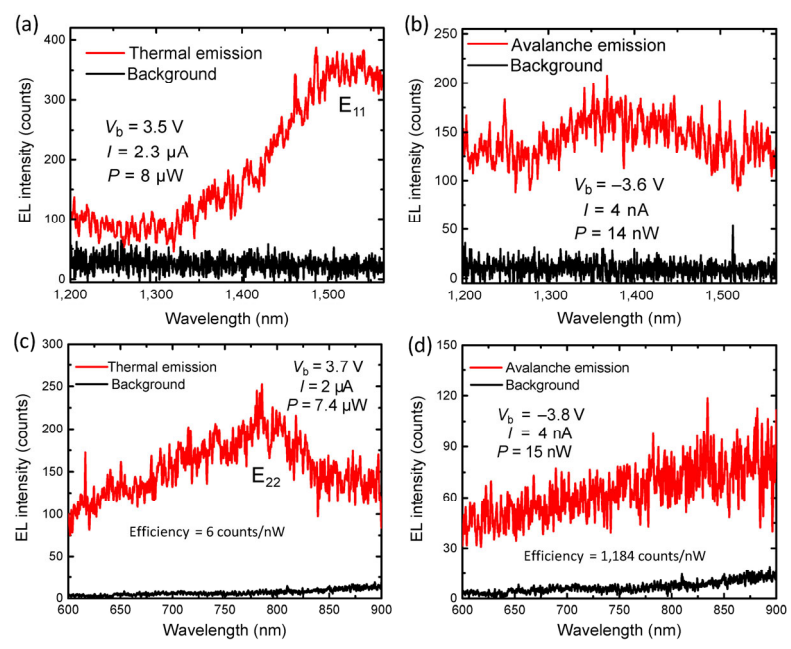


Figure 3 (a) Spectrum of thermal emission taken at $V_b = 3.5$ V and $I_b = 2.3$ μA, and (b) spectrum of sub-avalanche light emission taken at $V_b = -3.6$ V and $I_b = 4$ nA from a suspended dual-gate CNT FET device. Spectra collected from another device within the visible wavelength range of (c) thermal emission taken at $V_b = 3.7$ V and $I_b = 2$ μA, and (d) sub-avalanche light emission taken at $V_b = -3.8$ V and $I_b = 4$ nA.

Acknowledgements

The authors would like to acknowledge support from the Northrop Grumman-Institute of Optical Nanomaterials and Nanophotonics (NG-ION²) (B. W.). This research was supported by the NSF Award No. CBET-1905357 (S. Y.) and Department of Energy DOE Award No. DE-FG02-07ER46376 (Y. W.). R. K. acknowledges funding from AFOSR Grant No. FA9550-16-1-0306 and National Science Foundation Award No. 1610604. R. A. acknowledges a USC Provost Graduate Fellowship. A portion of this work was carried out in the University of California Santa Barbara (UCSB) nanofabrication facility. This work was also carried out in part at the Center for Integrated Nanotechnologies, a U.S. Department of Energy, Office of Science user facility, Y. L., S. K. D., and H. H. acknowledge partial support of the LANL LDRD program and Y. L. and H. H. acknowledge support from DOE BES FWP# LANLBES22.

Electronic Supplementary Material: Supplementary Material (Figure S1 shows PL spectra taken from two representative dual-gate CNT FETs exhibiting spectral features corresponding to the E₁₁ exciton. Figure S2 shows calculated conduction and valence band profiles of a dual-gate CNT FET device under forward and reverse bias conditions) is available in the online version of this article at https://doi.org/10.1007/s12274-020-2941-3.

References

- Ghosh, S.; Bachilo, S. M.; Simonette, R. A.; Beckingham, K. M.; Weisman, R. B. Oxygen doping modifies near-infrared band gaps in fluorescent single-walled carbon nanotubes. Science 2010, 330, 1656-1659
- Miyauchi, Y.; Iwamura, M.; Mouri, S.; Kawazoe, T.; Ohtsu, M.; Matsuda, K. Brightening of excitons in carbon nanotubes on dimensionality modification. Nat. Photonics 2013, 7, 715-719.
- Ma, X. D.; Adamska, L.; Yamaguchi, H.; Yalcin, S. E.; Tretiak, S.; Doorn, S. K.; Htoon, H. Electronic structure and chemical nature of oxygen dopant states in carbon nanotubes. ACS Nano 2014, 8, 10782-10789
- Ma, X. D.; Hartmann, N. F.; Baldwin, J. K. S.; Doorn, S. K.; Htoon, H. Room-temperature single-photon generation from solitary dopants of carbon nanotubes. Nat. Nanotechnol. 2015, 10, 671-675.
- Ma, X. D.; Baldwin, J. K. S.; Hartmann, N. F.; Doorn, S. K.; Htoon, H. Solid-state approach for fabrication of photostable, oxygen-doped carbon nanotubes. Adv. Fuct. Mater. 2015, 25, 6157-6164.
- [6] Ma, X. D.; James, A. R.; Hartmann, N. F.; Baldwin, J. K.; Dominguez, J.; Sinclair, M. B.; Luk, T. S.; Wolf, O.; Liu, S.; Doorn, S. K. et al. Solitary oxygen dopant emission from carbon nanotubes modified by dielectric metasurfaces. ACS Nano 2017, 11, 6431-6439.
- [7] Matsunaga, R.; Matsuda, K.; Kanemitsu, Y. Observation of charged excitons in hole-doped carbon nanotubes using photoluminescence and absorption spectroscopy. Phys. Rev. Lett. 2011, 106, 037404.
- Yuma, B.; Berciaud, S.; Besbas, J.; Shaver, J.; Santos, S.; Ghosh, S.; Weisman, R. B.; Cognet, L.; Gallart, M.; Ziegler, M. et al. Biexciton, single carrier, and trion generation dynamics in single-walled carbon nanotubes. Phys. Rev. B 2013, 87, 205412.
- Högele, A.; Galland, C.; Winger, M.; Imamoğlu, A. Photon antibunching in the photoluminescence spectra of a single carbon nanotube. Phys. Rev. Lett. 2008, 100, 217401.
- [10] He, X. W.; Hartmann, N. F.; Ma, X. D.; Kim, Y.; Ihly, R.; Blackburn, J. L.; Gao, W. L.; Kono, J.; Yomogida, Y.; Hirano, A. et al. Tunable room-temperature single-photon emission at telecom wavelengths from sp³ defects in carbon nanotubes. Nat. Photonics 2017, 11,
- [11] Ju, S. Y.; Kopcha, W. P.; Papadimitrakopoulos, F. Brightly fluorescent single-walled carbon nanotubes via an oxygen-excluding surfactant organization. Science 2009, 323, 1319-1323.

- [12] Ishii, A.; Uda, T.; Kato, Y. K. Room-temperature single-photon emission from micrometer-long air-suspended carbon nanotubes. Phys. Rev. Appl. 2017, 8, 054039.
- [13] Hofmann, M. S.; Glückert, J. T.; Noé, J.; Bourjau, C.; Dehmel, R.; Högele, A. Bright, long-lived and coherent excitons in carbon nanotube quantum dots. Nat. Nanotechnol. 2013, 8, 502-505.
- [14] Walden-Newman, W.; Sarpkaya, I.; Strauf, S. Quantum light signatures and nanosecond spectral diffusion from cavity-embedded carbon nanotubes. Nano Lett. 2012, 12, 1934-1941.
- Mueller, T.; Kinoshita, M.; Steiner, M.; Perebeinos, V.; Bol, A. A.; Farmer, D. B.; Avouris, P. Efficient narrow-band light emission from a single carbon nanotube p-n diode. Nat. Nanotechnol. 2010, 5,
- [16] Misewich, J. A.; Martel, R.; Avouris; Tsang, J. C.; Heinze, S.; Tersoff, J. Electrically induced optical emission from a carbon nanotube FET. Science 2003, 300, 783-786.
- [17] Freitag, M.; Perebeinos, V.; Chen, J.; Stein, A.; Tsang, J. C.; Misewich, J. A.; Martel, R.; Avouris, P. Hot carrier electroluminescence from a single carbon nanotube. Nano Lett. 2004, 4, 1063-1066.
- [18] Chen, J.; Perebeinos, V.; Freitag, M.; Tsang, J.; Fu, Q.; Liu, J.; Avouris, P. Bright infrared emission from electrically induced excitons in carbon nanotubes. Science 2005, 310, 1171-1174.
- [19] Pfeiffer, M. H. P.; Stürzl, N.; Marquardt, C. W.; Engel, M.; Dehm, S.; Hennrich, F.; Kappes, M. M.; Lemmer, U.; Krupke, R. Electroluminescence from chirality-sorted (9.7)-semiconducting carbon nanotube devices. Opt. Express 2011, 19, A1184-A1189.
- [20] Liu, Z. W.; Bushmaker, A.; Aykol, M.; Cronin, S. B. Thermal emission spectra from individual suspended carbon nanotubes. ACS Nano 2011, 5, 4634-4640.
- [21] Wang, B.; Rezaeifar, F.; Chen, J. H.; Yang, S. S.; Kapadia, R.; Cronin, S. B. Avalanche photoemission in suspended carbon nanotubes: Light without Heat. ACS Photonics 2017, 4, 2706-2710.
- [22] Wang, B.; Yang, S. S.; Shen, L.; Cronin, S. B. Ultra-low power light emission via avalanche and sub-avalanche breakdown in suspended carbon nanotubes. ACS Photonics 2018, 5, 4432-4436.
- [23] Bushmaker, A. W.; Deshpande, V. V.; Bockrath, M. W.; Cronin, S. B. Direct observation of mode selective electron-phonon coupling in suspended carbon nanotubes. Nano Lett. 2007, 7, 3618-3622.
- [24] Hsu, I. K.; Pettes, M. T.; Aykol, M.; Shi, L.; Cronin, S. B. The effect of gas environment on electrical heating in suspended carbon nanotubes. J. Appl. Phys. 2010, 108, 084307.
- [25] Amer, M.; Bushmaker, A.; Cronin, S. Anomalous kink behavior in the current-voltage characteristics of suspended carbon nanotubes. Nano Res. 2012, 5, 172-180.
- [26] Bushmaker, A. W.; Deshpande, V. V.; Hsieh, S.; Bockrath, M. W.; Cronin, S. B. Direct observation of born-oppenheimer approximation breakdown in carbon nanotubes. Nano Lett. 2009, 9, 607–611.
- [27] Bushmaker, A. W.; Deshpande, V. V.; Hsieh, S.; Bockrath, M. W.; Cronin, S. B. Large modulations in the intensity of Raman-scattered light from pristine carbon nanotubes. Phys. Rev. Lett. 2009, 103, 067401.
- [28] Chang, S. W.; Theiss, J.; Hazra, J.; Aykol, M.; Kapadia, R.; Cronin, S. B. Photocurrent spectroscopy of exciton and free particle optical transitions in suspended carbon nanotube pn-junctions. Appl. Phys. Lett. 2015, 107, 053107.
- [29] Deshpande, V. V.; Chandra, B.; Caldwell, R.; Novikov, D. S.; Hone, J.; Bockrath, M. Mott insulating state in ultraclean carbon nanotubes. Science 2009, 323, 106-110.
- [30] Wang, B.; Yang, S. S.; Wang, Y.; Ahsan, R.; He, X. W.; Kim, Y.; Htoon, H.; Kapadia, R.; John, D. D.; Thibeault, B. et al. Auger suppression of incandescence in individual suspended carbon nanotube pn-junctions. ACS Appl. Mater. Interfaces 2020, 12, 11907–11912.
- [31] Chang, S. W.; Bergemann, K.; Dhall, R.; Zimmerman, J.; Forrest, S.; Cronin, S. B. Nonideal diode behavior and bandgap renormalization in carbon nanotube p-n junctions. IEEE Trans. Nanotechnol. 2014, 13, 41-45.
- [32] Freitag, M.; Steiner, M.; Naumov, A.; Small, J. P.; Bol, A. A.; Perebeinos, V.; Avouris, P. Carbon nanotube photo- and electroluminescence in longitudinal electric fields. ACS Nano 2009, 3, 3744-3748.

- [33] Steiner, M.; Freitag, M.; Perebeinos, V.; Naumov, A.; Small, J. P.; Bol, A. A.; Avouris, P. Gate-variable light absorption and emission in a semiconducting carbon nanotube. *Nano Lett.* 2009, 9, 3477–3481.
- [34] Yasukochi, S.; Murai, T.; Moritsubo, S.; Shimada, T.; Chiashi, S.; Maruyama, S.; Kato, Y. K. Gate-induced blueshift and quenching of photoluminescence in suspended single-walled carbon nanotubes. *Phys. Rev. B* 2011, 84, 121409.
- [35] Yoshida, M.; Popert, A.; Kato, Y. K. Gate-voltage induced trions in suspended carbon nanotubes. *Phys. Rev. B* 2016, 93, 041402.
- [36] Chynoweth, A. G.; McKay, K. G. Photon emission from avalanche breakdown in silicon. *Phys. Rev.* 1956, 102, 369–376.
- [37] Van Drieënhuizen, B. P.; Wolffenbuttel, R. F. Optocoupler based on the avalanche light emission in silicon. *Sens. Actuators A: Phys.* **1992**, *31*, 229–240.

Reproduced with permission of copyright owner. Further reproduction prohibited without permission.